Experimental and theoretical analysis of H-bonded supramolecular assemblies of PTCDA molecules

M. Mura,[1] X. Sun,[2] F. Silly,[2,3,4,5,*] H. T. Jonkman,[2] G. A. D. Briggs,[3] M. R. Castell,[3] and L. N. Kantorovich[1,†]
[1]*Physics, King's College London, The Strand, London WC2R 2LS, United Kingdom*
[2]*Zernike Institute for Advanced Materials, University of Groningen, Nijenborgh 4, NL-9747 AG Groningen, The Netherlands*
[3]*Department of Materials, University of Oxford, Parks Road, Oxford OX1 3PH, United Kingdom*
[4]*CEA, IRAMIS, SPCSI, F-91191 Gif-sur-Yvette, France*
[5]*UPMC, IPCM, UMR CNRS 7201, 4 Place Jussieu, 75005 Paris, France*
(Received 4 January 2010; revised manuscript received 25 February 2010; published 7 May 2010)

Using a systematic method based on considering all possible hydrogen bond connections between molecules and subsequent density-functional theory (DFT) calculations, we investigated planar superstructures that the perylene-3,4,9,10-tetracarboxylic-3,4,9,10-dianhydride (PTCDA) molecules can form in one and two dimensions. Structures studied are mostly based on two molecule unit cells and all assemble in flat periodic arrays. We show that 42 different monolayer structures are possible, which can be split into eight families of distinct structures. A single representative of every family was selected and relaxed using DFT. We find square, herringbone and brick wall phases (among others) which were already observed on various substrates. Using scanning tunneling microscopy in ultrahigh vacuum, we also observed herringbone and square phases after sublimation of PTCDA molecules on the Au(111) surface at room temperature, the square phase being observed for the first time on this substrate. The square phase appears as a thin stripe separating two herringbone domains and provides a perfect structural matching for them. A similar structural formation serving as a domain wall between two other phases has been recently reported on the same surface formed by melamine molecules [F. Silly *et al.*, J. Phys. Chem. C **112**, 11476 (2008)]. Our theoretical analysis helps to account for these and other observed complex structures.

DOI: 10.1103/PhysRevB.81.195412 PACS number(s): 68.37.Ef, 31.15.E−, 81.16.Fg

I. INTRODUCTION

Organic molecules can form structures on metallic and other inorganic surfaces.[1–12] Some organic molecules have the ability to self-assemble in two-dimensional (2D) networks when they are deposited on a surface. Some properties of these templates, such as their possibility to form either chiral or non-chiral ordered structures,[13,14] have been intensively studied for understanding their possible applications in nanotechnology (e.g., Refs. 15–18).

Perylene-3, 4, 9, 10-tetracarboxylic-3, 4, 9, 10-dianhydride (PTCDA) is an archetypal organic semiconducting molecule which is a potential building block for the realization of organic electronic devices.[19] PTCDA molecules are of special interest in engineering of 2D supramolecular nanostructures and thin films due to their special rectangular shape (Fig. 1) and a specific hydrogen-bonding functionality. These long molecules have been employed, combined with other molecules such as melamine,[20] 4,4″ diamino-p-terphenyl (DATP) and 2,4,6-tris(4-aminophenyl)-1,3,5-triazine (TAPT),[21] as building blocks for obtaining sophisticated 2D supramolecular structures. Perylene derivative molecules are one of the promising candidates for engineering organic architectures, or templates, designed for trapping foreign molecules (e.g., fullerenes Refs. 6, 10, and 22–31). Assessing and controlling PTCDA assemblies are of technological interest for optimizing the design of organic thin film electronic devices as it has been shown that the exciton diffusion length of PTCDA is affected by crystalline order.[32]

The self-assembled structures which the molecules form on surfaces depend on the nature of the molecules as well the surface preparation, the deposition rate and the temperature. PTCDA molecules have been deposited on different substrates such as metallic Cu(110),[33] Cu(111),[34] Ag(110),[35] Ag(111),[35,36] Au(100),[37] Au(788) (Ref. 38) and Au(111),[20,37–42] nonmetallic KBr(001),[43,44] NaCl,[45,46] on graphene layers,[47–49] GaAs(001),[50] Si/Ag(111),[24] and mica.[51] Four structures formed by PTCDA molecules have been observed so far: (i) herringbone,[20,24,34–38,41–44] (ii) square,[24,33,37,38,41] (iii) brick wall,[35,47] and (iv) a more complex hexagonal phase[24] which can be considered as a combination of a herringbone and square phases.

After deposition of PTCDA molecules on the Au(111) surface, we observed using scanning tunneling microscopy (STM) (Refs. 52 and 53) all these previously reported structures. In addition to these, we discovered a new complex assembly, which can be described as a narrow band of a

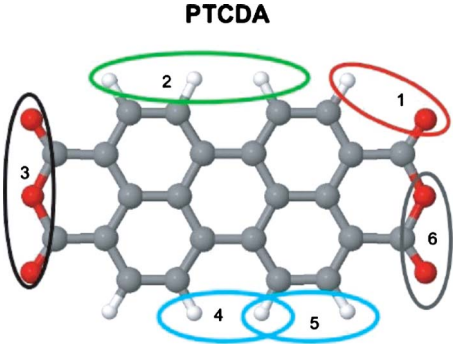

FIG. 1. (Color online) PTCDA molecule and its nonequivalent binding sites shown by numbered ovals.

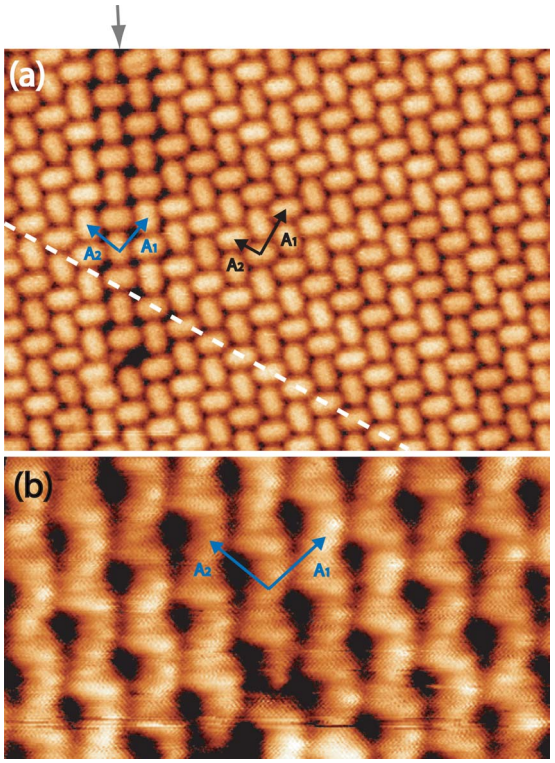

FIG. 2. (Color online) STM images of the new PTCDA networks on the Au(111) surface. (a) The narrow stripe of the square phase provides a buffer for two shifted herringbone phases on the left and right of it. The black arrow at the top of the image indicates the square phase. The lattice vectors of the square and herringbone phases are explicitly indicated by blue and black arrows, respectively. The scanned area is 210×150 Å^2. The tunneling current $I_t = 0.3$ nA and the applied voltage $V_s = 1.5$ V. (b) The domino phase; the lattice vectors are indicated by the blue arrows. The scanned area is 105×70 Å^2. The tunneling current $I_t = 0.7$ nA and the applied voltage $V_s = -0.3$ V.

square phase incorporated between two extended herringbone phases, Fig. 2. The two herringbone phases are shifted with respect to each other. The square phase between them, as we shall demonstrate, serves as a domain wall similar to previous observations of an intermediate phase providing the matching between two melamine phases on gold.[54]

By using techniques such as STM and atomic force microscopy (AFM),[55] it is possible to characterize the formation of nanostructures with well defined properties. A complementing theoretical approach is required to account for the geometries of observed structures. In this study we investigate the possible structures that PTCDA molecules can form on a flat metal surface such as Au(111), using density-functional theory (DFT). In order to consider all possible structures these molecules can form, we use a systematic approach developed earlier for adenine,[56] melamine,[57] and PTCDI.[58] This previous work also demonstrated how the symmetry of molecules may affect the number of monolayers they are able to form: we show that the number of possible structures these rather symmetric molecules can form with each other is significantly limited.

Our theoretical analysis explains all structures already observed on various substrates. In addition, other structures are also predicted. We also stress that more structures are possible if one applies our method with appropriate restrictions. In particular, as we shall see, a complex hexagonal phase[24] found on the Si/Ag(111) surface and the domain wall assembly found in our experiments on the Au(111) surface, can be easily rationalized.

The plan of this paper is as follows. In Sec. II we briefly outline the theoretical and experimental methods used. Our STM observations and the corresponding theoretical analysis of possible PTCDA structures are discussed in Sec. III. Finally, conclusions are given in Sec. IV.

II. METHODS

A brief outline of experimental and theoretical methods used in this study is given here.

A. Experimental

As a substrate, we used Au(111) films grown on mica. The samples were introduced into the ultrahigh vacuum (UHV) chamber of an STM apparatus (JEOL JSTM4500S and Omicron VT AFM-STM with Nanonis controler) operating at a pressure of 10^{-8} Pa. The Au(111) surfaces were sputtered with Ar^+ ions and then annealed in UHV at temperatures between 600°C and 800 °C, typically for 30 min. PTCDA molecules were evaporated at 270 °C and then deposited on the gold surface kept at room temperature. The samples were not post-annealed after molecular deposition. Etched tungsten and cut Pt/Ir tips were used to obtain constant current STM images at room temperature with a bias voltage applied to the sample. STM images were processed and analyzed using the home made FabViewer application.[59]

B. Theoretical

Here we describe our systematic approach to construct the supramolecular structures and then briefly explain the computational method used. All our calculations are for a two-dimensional gas and neglect explicitly their interaction with the substrate. In order to construct all possible structures, a systematic approach described in the previous work[56–58] was used consisting of the following steps: (i) identification of all peripheral binding sites the molecule has that can participate in a hydrogen bonding with another molecule; (ii) construct all possible dimers; (iii) by connecting molecules, using dimer rules, all possible unit cells are constructed having a predefined number of molecules; (iv) all possible chains (i.e., one-dimensional structures) are built for every unit cell; (v) by attaching chains parallel to each other, all possible 2D periodic structures are formed; (vi) stabilities of the predicted in this way assemblies are estimated by summing up all dimer energies (per cell) and, (vii) the most stable predicted structures are then fully relaxed using an *ab initio* method to finally obtain their geometries and binding energies.

The calculations were performed using the *ab initio* SIESTA method,[60,61] which is based on a localized numerical orbital basis set, periodic boundary conditions, and the first principles scalar-relativistic norm-conserving Troullier-Martins[62] pseudopotential factorized in the

Kleinman-Bylander[63] form. We used the Perdew, Becke and Ernzerhof (PBE) (Ref. 64) generalized gradient approximation for the exchange and correlation which was found previously to be adequate in representing hydrogen bonding between DNA base molecules.[65] In each calculation, atomic relaxation was performed until forces on atoms were less than 0.01 eV/Å in the cases of dimers and 0.03 eV/Å in the cases of monolayers.

A number of energies are worked out and used in the analysis. First, the stabilization energy, E_{stab}, is defined as the total energy of the relaxed combined system (e.g., the PTCDA dimer) minus the total energies of all its individual components (two PTCDA molecules) relaxed separately. The basis set superposition error (BSSE) correction must be applied to this energy to account for the fact that the localized basis set is used; the counterpoise methods has been used here to correct for this.[66] The system is considered stable if $E_{\mathrm{stab}}<0$. To characterize the interaction between the two parts of a composite system (e.g., a pair), the interaction energy, E_{int}, is used, which is defined as the energy of the pair minus the energy of each individual molecule calculated in the geometry of the pair (i.e., without relaxation); this energy is always negative for a stable system. Finally, the deformation energy, E_{def}, characterizes energies lost by each part of the combined system (e.g., the two molecules of the pair) due to their subsequent relaxation. It is calculated as a sum of differences between the energies of individual molecules in the combined system and their relaxed energies when they are completely separated (at infinity), E_{i0}

$$E_{\mathrm{def}}=\sum_{i}(E_i-E_{i0}). \tag{1}$$

The interaction and deformation energies, as defined above, must sum up exactly to the stabilization energy, i.e., $E_{\mathrm{stab}}=E_{\mathrm{int}}+E_{\mathrm{def}}$. In this way, one can see how the deformation energy is compensated by the interaction energy if the structure is indeed stable. Note, however, that this relationship would only be exact if plane waves were used in our DFT calculations. Since, we use SIESTA which employs a localized basis set this relationship would only be exact *prior* to the application of the BSSE correction. Therefore, to simplify the analysis, the same BSSE correction was applied to the interaction and stabilization energies ensuring that this exact relationship remains.

The simplest system we consider is a PTCDA dimer. When studying however more complex systems such as e.g., molecular chains [one-dimensional (1D)] or monolayers (2D), each molecule is bound to more than one other molecule. Each hydrogen bonding between two molecules may result in some redistribution of the electron density around other binding sites not involved in the H bonding in question. However, these other binding sites may be used to bind additional molecules, and hence the mentioned density redistribution may affect the ability of the molecules to form complex systems containing more than two molecules via hydrogen bonding. This, the so-called *resonance assisted hydrogen bonding* (RAHB) effect, is known to play a role in some systems stabilized by hydrogen bonding.[56,57,67,68] To characterize this collective effect, it is convenient to perform also an approximate calculation in which the binding energy of the whole complex system is "estimated" as a simple sum of binding energies of each pair of molecules involved. If for instance the DFT calculated binding energy of the whole system is lower (more negative) than the sum of dimer binding energies, then this would indicate on the existence of the *positive* RAHB effect, i.e., that the hydrogen bonds effect favorably each other in the system.

The stabilization energy gives an indication of the strength of the hydrogen bonds in the system. The relaxed geometry also provides an indirect indication about the stability of the hydrogen bonds enabled in the structure: the latter often prefer planar configurations and there are preferential values in the hydrogen bonds of the donor-H-acceptor distances and of the angle associated with them;[56,65] a general rule is that hydrogen bonds try to become as linear as possible with the acceptor-H-donor distance, depending on the actual acceptors involved, being within the range of 2.6–3.0 Å.

Another way of characterizing the strength of the hydrogen bonding between e.g., two molecules is by analyzing the electron density difference plots.[54,56,57,65,69,70] These are obtained by subtracting from the electron density of the combined system (e.g., a dimer) the densities of each of its individual components (the two molecules) calculated in the geometry of the combined system. This way one can see a redistribution of the electron density due to e.g., formation of chemical bonds between the components of the combined system. Hydrogen bonds were found to display a so-called kebab structure of alternating regions of charge excess and depletion that represents the redistribution of the charge density due to the hydrogen bond formation.[65] The stronger the bond, the more regular the kebab structure is. This concept can easily be generalized for complexes containing more than two molecules, and we shall show examples of this analysis as well.

III. SUPRAMOLECULAR ASSEMBLIES OF PTCDA MOLECULES

A. STM observations

After deposition of PTCDA molecules on the Au(111) surface, as explained in Sec. II A, we did not observe any single PTCDA molecules. That means that they diffuse very fast at room temperature spontaneously forming domains of well-known square, herringbone, and brick wall arrangements. The herringbone phase appears more often than the others. It is seen in the left and right parts of Fig. 2(a). These two appearances of the herringbone phase are shifted in phase: if one continues a row on the right of equally tilted molecules (see the white dashed line in the image), the row eventually meets the edges of two rows of molecules on the left with opposite tilting, see Fig. 2(a). In order to facilitate the continuation of the assembly, a narrow stripe of the square phase is visible [indicated by the black arrow at the top of the image Fig. 2(a)] which allows the perfect matching between the two shifted herringbone domains. The PTCDA rows of the two domains are shifted by 1/4 of the lattice vector A_1 in the direction nearly perpendicular to the row direction; $\mathbf{A}_1$ is

the longer vector in Fig. 2 for the herringbone phase. Interestingly, the herringbone phase is seen to continue at the bottom of the square stripe where a defect (a molecule "vacancy" accompanied by some additional disorder nearby) can be observed which probably facilitates the growth of the square phase.

Also a new PTCDA arrangement has been observed [Fig. 2(b)], the "domino" phase. In the domino phase the molecules are arranged in squares, each square is made out of four molecules attached to each other as domino pieces, see Fig. 2(b).

The observed lengths of the lattice vectors, the angle between them γ, as well the angle τ between two molecules in the unit cell (both in degrees) for the three structures were measured to be: (i) herringbone: $A_1=19.4$ Å, $A_2=12.5$ Å, $\gamma=88°$, and $\tau=85°$; (ii) square: $A_1=16.5$ Å, $A_2=16.2$ Å, $\gamma=89°$, and $\tau=88°$; (iii) domino: $A_1=15.5$ Å, $A_2=15.3$ Å, $\gamma=105°$, and $\tau=90°$.

B. Interaction of PTCDA molecules with the gold surface

High mobility of individual PTCDA molecules on the Au(111) surface suggests that the potential energy surface (PES) of the molecules on this particular surface is very flat. This conclusion is confirmed by other STM studies related to different flat organic molecules such as DNA bases,[71,72] melamine,[54,73] and cyanuric acid[73] deposited on the same Au(111) surface. These molecules demonstrated a very high mobility on the surface at room temperature, so that STM images were taken at much lower temperatures to stabilize them, e.g., 150 K for the adenine network and in the range of 100–160 K for the melamine and cyanuric acid on the same surface.[71–73]

Recent extensive DFT calculations with the PBE density functional[74] revealed that the PES of a PTCDA molecule on the Au(111) surface is indeed flat, with the corrugation never exceeding 0.04 eV. Thus, these DFT calculations suggest that the molecules can freely move across the gold surface at room temperature, i.e., during their deposition, and hence can form molecular assemblies spontaneously at this temperature. However, these calculations also showed an important deficiency of the PBE density functional in that the calculated adsorption energy of around 0.17 eV appears to be an order of magnitude smaller than the measured value of 2.0 eV.[75]

The weak binding of the molecule to the gold surface is due to the well-known problem of the most density functional, including the PBE, which is the lack of the dispersion [or van der Waals (vdW)] interaction. This point has been thoroughly investigated in a recent study[74] where two methods have been used to assess the role played by the vdW forces in binding of some flat organic molecules, including the PTCDA, to the Au(111) surface. In the first method a classical force field[76] implemented in the Sci-Fi code[77] was used, while in the second method the *ab initio* fully self-consistent vdW-DF method[78] was employed as implemented in the SIESTA code.[79] Both methods came essentially to the same conclusions: (i) the molecule lies flat on the surface at the distance of 3.0 Å (classical) and 3.3 Å (vdW-DF) from it; (ii) the dispersion interaction provides the main binding mechanism with significant adsorption energies of −1.88 and −2.03 eV for vdW-DF and the force-field methods, respectively; (iii) the PES of the molecule on the gold surface is extremely flat, with the corrugation not exceeding 0.05 eV similarly to the PBE results. An adsorption of a melamine dimer on the Au(111) surface was also considered in Ref. 74 using the vdW-DF method, and it was concluded that the hydrogen bonding between melamine molecules on this surface is not severely affected by it. We believe it is reasonable to extend this conclusion to the hydrogen bonding of other flat molecules on gold, including PTCDA. These results are in complete agreement with the STM observations on the molecules mobility[68,71,80–82] and the measured high adsorption energy.[75]

We also note that the vdW-DF calculations also revealed that there is no charge transfer between the molecule and the surface; this was confirmed by both the electronic charge density and the projected density of states analyses. This finding partially explains the flatness of the PES.

Summarizing, one may say that, due to an extremely small corrugation of the surface potential, the main effect of the gold surface is in keeping the molecules on it without restricting their lateral movement. In a way, the molecules are constrained in a 2D "pool" at a distance of about 3.3 Å from the surface.[74] Therefore, one can model various assemblies of the PTCDA molecules on the Au(111) surface by considering all their planar (2D) arrangements, i.e., without directly accounting for their interaction with the surface. In other words, these results imply that the *gas-phase* modeling, at least as the first approximation, should be adequate.

C. Two-dimensional PTCDA structures in the gas phase

In this section, we shall consider our theoretical method in application to all possible gas-phase periodic structures formed by PTCDA molecules. All structures based on two molecules per unit cell will be described in more detail first. Then we shall discuss what one can expect when going beyond this limitation. We start by describing in detail the approach used and shall present the PTCDA dimers; this will then be followed by building all superstructures.

1. PTCDA dimers

The starting point in our analysis is the identification of the binding sites in the PTCDA molecule, see Fig. 1. Six possible non-equivalent binding sites have been identified. Sites 2, 4, and 5 are exclusively of donor type; they are composed of carbon-hydrogen groups and are able to form either double or triple hydrogen bonds. Two of the binding sites are exclusively acceptors (3 and 6) and are composed by oxygens enabling them to form three or two hydrogen bonds as well. There is also a third kind of the binding site (site 1) with both donor and acceptor atoms (it is composed of an oxygen and hydrogen atoms able to form a double hydrogen bond); there are four such bonds along the molecule perimeter.

Although, the PTCDA molecule has many, both different and similar, binding sites, only a limited number of distin-

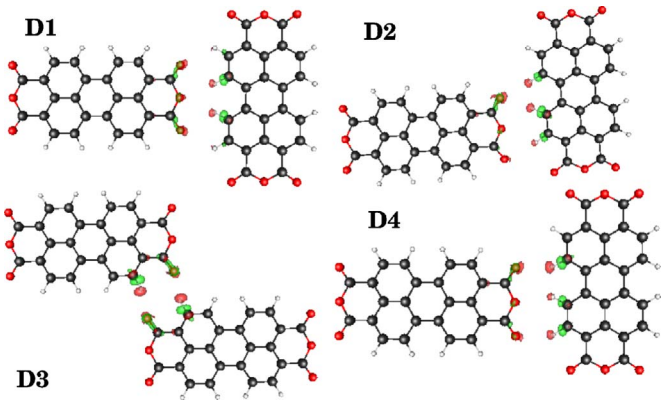

FIG. 3. (Color online) The geometries of the four possible PTCDA dimers shown together with the electron density difference plots corresponding to ± 0.01 Å^{-3}. The green surfaces correspond to the regions of positive electron density difference (excess) and the red areas correspond to the regions of negative electron density difference (depletion).

guishable dimers are possible due to the symmetry of the molecule. Combining two PTCDA molecules, four dimers are obtained as shown in Fig. 3. Three of these dimers (D1, D2, and D4) are very similar, as they are constructed by placing one PTCDA molecule perpendicular to the other and shifting along its longer side. Dimer D1 is formed by aligning two hydrogen atoms in the center of the long side of one molecule with the three oxygens of the other. Dimers D2 and D4 are obtained by shifting the molecules with respect to each other as compared with the D1 configuration. The final dimer structure D3 is obtained when the two PTCDA molecules are connected in a "head-and-tail" like structure, see Fig. 3, using the binding site 1.

The four dimers are found to relax into stable planar geometries. As expected, the stabilization energies of the dimers shown in Table I, are found to be rather small and similar; this also means that it could be energetically easy to transform between the D1, D2, and D4 dimers. In the cases of similar D1, D2, and D4 dimers all three oxygens of one molecule participate, however, a different number of hydrogen atoms (between 2 and 3) participate in the other.

As evidenced by the electron density difference plots in Fig. 3 and the binding energies, in all cases the dimers are weakly bonded. By a small margin, the most stable dimer is D4, remaining still very weak. This is peculiar since the most developed "kebab" structure is displayed by the dimer D3. Apparently the dimer D4 in the end appears to be marginally stronger due to the overall effect of having three (weak) hydrogen bonds.

TABLE I. Stabilization, interaction, deformation, and BSSE energies (in eV) of the four PTCDA dimers. The stabilization and interaction energies include the BSSE correction in each case.

Index	D1	D2	D3	D4
E_{stab}	−0.25	−0.23	−0.26	−0.27
E_{def}	0.01	0.01	0.02	0.02
E_{int}	−0.26	−0.24	−0.28	−0.29
E_{BSSE}	0.10	0.08	0.13	0.08

One would expect stronger hydrogen bonds when the oxygen is involved due to its high electronegativity, however, from the chemical point of view, in all cases the hydrogen donors are carbon atoms that are not enough electronegative to contribute sufficiently into the hydrogen bond formation. Small deformation energies E_{def}, shown in Table I, underline the rigidity of the PTCDA molecule, including its C-H groups.

Once all the possible dimers are constructed, the next step is to identify the binding sites available to connect the PTCDA dimers into a 1D chain. In the next section the possible chains based on the PTCDA pairs are presented.

2. One-dimensional chains based on the PTCDA pairs

In this subsection we present the 1D structures that can be built using a PTCDA dimer as a unit cell. As before, we start from the identification of the binding sites available on the periphery of the dimer and, see Fig. 3, for the connection with more dimers. We build 1D chains by connecting dimers in a chain-like manner along one direction. The chains are obtained by adding a second dimer to a certain binding site of the first dimer, then a third dimer is added to the same site of the second one, and so on. In this way, by using free dimer binding sites 30 different chains can be constructed. However, as many chains are geometrically similar (mainly due to similarity of the dimers D1, D2, and D4), one can group them into families of the geometrically similar chains and then calculate the stabilization energy for a single representative of each of them. The PTCDA chains therefore were classified into distinct 10 families, and one chain from each family was selected and then calculated with DFT; their relaxed structures are presented here in Fig. 4 and the energies are given in Table II.

In the previous Sec. III C 1 we found that the PTCDA dimers are very close in energy. Therefore, it comes as no surprise that the calculated stabilization energies of chains constructed from them are also very close, spanning a narrow energy interval between −0.47 and −0.61 eV, i.e., the largest energy difference of only 0.14 eV is found here for the different chains, see Table II.

We have also presented in the Table II the evaluated stabilization energies, as described in Sec. II, which are sums (per unit cell) of the corresponding dimer energies. One can notice that the evaluated and the calculated (with DFT) stabilization energies are generally very close; small differences of up to −0.14 eV are found for some of the chains where there is an additional cooperative effect due to multiple hydrogen bonds, e.g., chain F9, see Fig. 4; chains F5 and F9 are the most stable ones. These chains are very similar in geometry, and have the maximum number of hydrogen and oxygen atoms involved in the chain formation.

The next step is to combine the chains and obtain all possible 2D structures.

3. Two-dimensional structures based on the PTCDA pairs

To build all possible 2D structures, we considered each chain separately and identified again the binding sites on

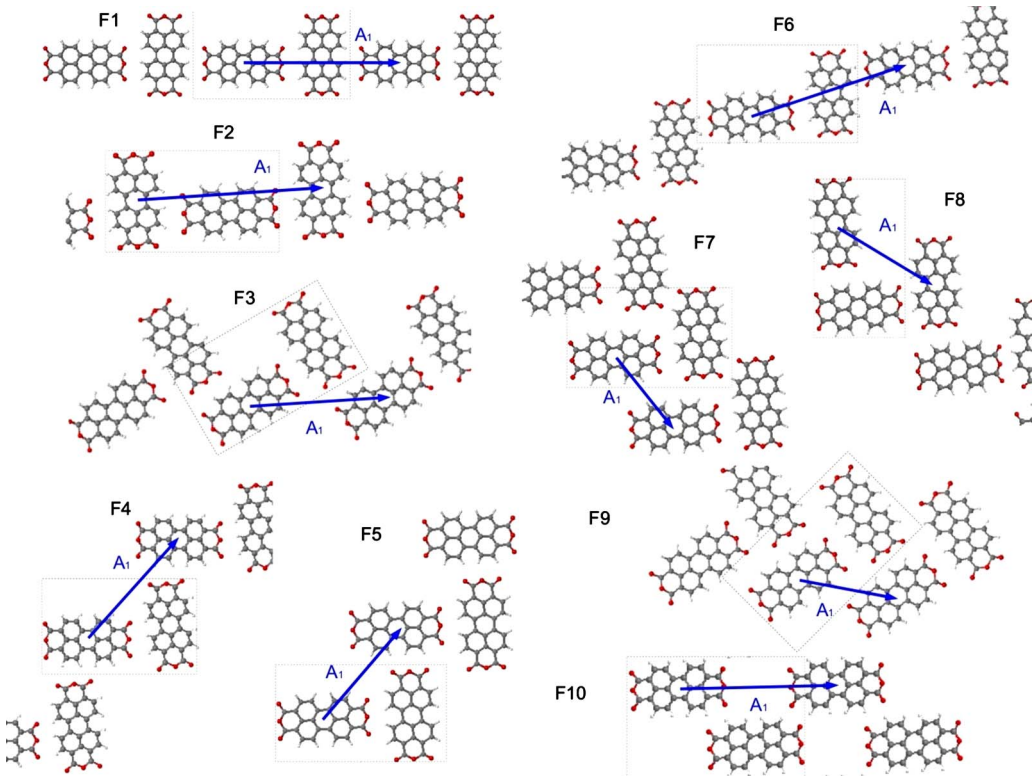

FIG. 4. (Color online) Relaxed geometries of the 10 PTCDA chains, named from F1 to F10 and representing 10 distinct families of chains. The lattice vector $\mathbf{A}_1$ is shown in all cases and the unit cell is indicated by a dashed box for convenience.

either side of the chain which are available to connect two chains. Out of 30 1D chains available (see Sec. III C 2), it is possible to generate 42 two-dimensional structures in which molecules are attached to each other via the PTCDA dimers connections. Such a large number of possible monolayers are due to a large number of dimers PTCDA molecules can form. However, because of a very similar nature of the dimers D1, D2, and D4, many monolayers look similar and their energetics and the structures are expected to be similar as well. Therefore, the same method as in the previous subsection has been used to simplify our discussion. Since we know all the dimer binding energies, the energy (per unit cell) of each monolayer can be evaluated by summing up all the relevant dimer energies. Then it is possible to classify the monolayers into families of similar monolayers taking into account both the geometry and the evaluated energy of each monolayer. In this way, eight families of monolayers have been identified and hence eight prototype (one from each family) monolayers have been considered for further DFT study. These eight representative structures, relaxed with our DFT method, together with the corresponding lattice vectors, are shown in Fig. 5. The structure MON8 is based on a single molecule in the unit cell; however, to simplify the forthcoming discussion, for this structure we consider a supercell with two molecules as indicated in Fig. 5.

We have also considered separately another monolayer MON9 shown in Fig. 6. Although this structure formally belongs to the second family of structures, it was found to be convenient to separate it out since it was found to be the best match for the domino phase observed in our STM image in Fig. 2(b).

The stabilization energies for the selected nine monolayers are given in Table III, while the density difference plots for three of them are shown in Fig. 7. The lattice vectors in each case are provided in Table V. The evaluated stabilization energies for monolayers MON1-MON4, MON6, and

TABLE II. The calculated (using SIESTA) and evaluated (as a sum of dimer energies) stabilization energies (in eV) of all ten PTCDA chains.

Index	F1	F2	F3	F4	F5
E_{stab} (calc.)	−0.47	−0.50	−0.56	−0.52	−0.60
E_{stab} (eval.)	−0.48	−0.50	−0.44	−0.44	−0.46
Index	F6	F7	F8	F9	F10
E_{stab} (calc.)	−0.56	−0.56	−0.48	−0.61	−0.48
E_{stab} (eval.)	−0.44	−0.50	−0.44	−0.50	−0.52

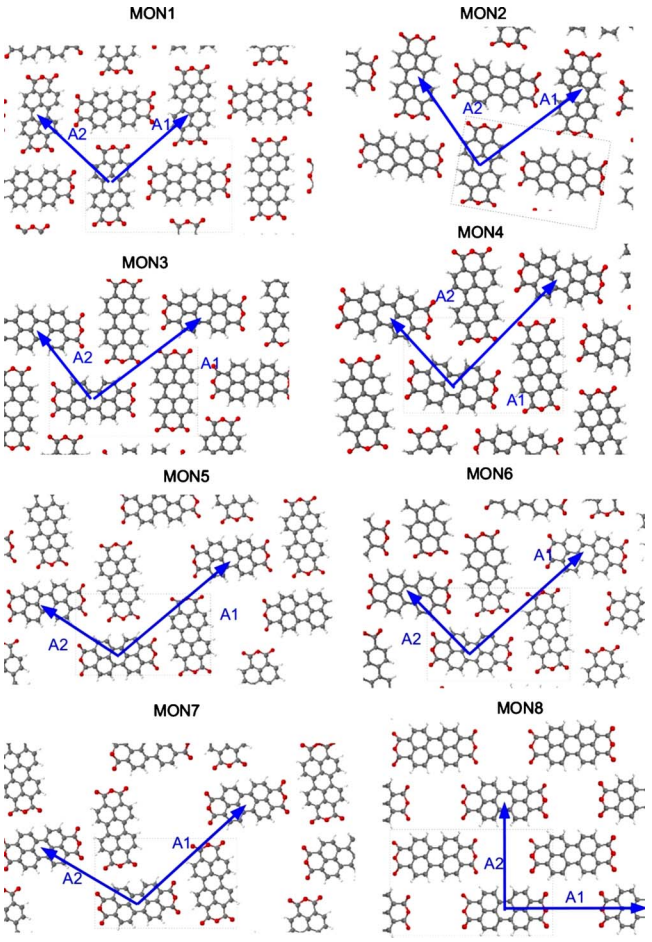

FIG. 5. (Color online) Eight PTCDA monolayers, representing eight distinct families of them, relaxed with our DFT method. Both the lattice vectors, $\mathbf{A}_1$ and $\mathbf{A}_2$, and the unit cell in each case are indicated.

MON9 based on PTCDA pairs are smaller than these calculated (with DFT). This is because the geometries changed after the relaxation with the DFT method and, at the same time, cooperative effects must be playing a role. The MON4 is the most stable monolayer and the extra stabilization energy can be explained as a result of the formation of additional hydrogen bonds in the structure, this is most clearly seen in the density difference plot in Fig. 7. The least stable monolayer is MON7 which density difference plot is also shown in Fig. 7 for comparison; in it every molecule has only three "contacts" with other molecules (which is less

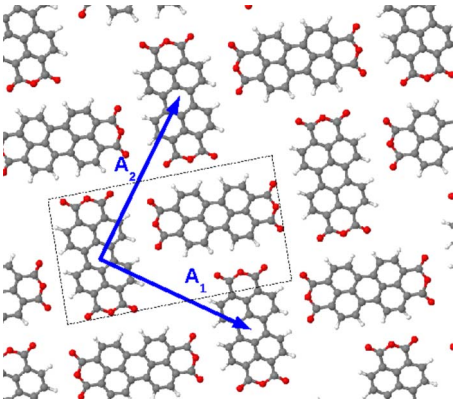

FIG. 6. (Color online) The monolayer MON9. Both the lattice vectors, $\mathbf{A}_1$ and $\mathbf{A}_2$, and the unit cell are indicated.

compared to the other structures) and the corresponding hydrogen bonds are very weak. As an example of a monolayer with intermediate stabilization energy, we show in Fig. 7 the density difference plot for MON1. One can see that each molecule is "connected" to four neighbors, however, all hydrogen bonds are rather weak.

The monolayer MON1 corresponds to the square phase observed experimentally,[24,33,37,38,41] MON2-MON7 monolayers present the herringbone phase,[20,24,34–38,41–44] while MON8 is the brick wall phase.[35,47] Lattice vectors of some of the observed monolayers on different substrates (defined in the same way as in Fig. 5) are shown in Table IV for comparison. The geometrical characteristics of the square and herringbone phases observed in this work (see Sec. III A) are also given. We see that some of our calculated gas-phase monolayers compare reasonably well with the experimental geometries, e.g., the square monolayer MON8 is very similar to the one observed on the Ag-terminated Si(111) surface.[24] We also observe in Fig. 5 and Table V a considerable variation of calculated possible herringbone phases (as is noticeable by differences in their lattice vectors and by the angle τ between the molecules in the unit cell) which comprise 6 families of structures. This variation is possible, in the first place, due to similarity of the D1, D2, and D4 dimer connections between PTCDA molecules in the perpendicular orientation. Monolayers MON3 and MON4 are similar to the observed ones in[20,24,35,43] and in this work, while monolayers MON5 and MON6 may be compared with the one observed in Ref. 34. The existence of different herringbone phases on the same surface is confirmed by experimental observations.[34,37,38,43]

TABLE III. The evaluated (by summing up dimer energies) and calculated (with DFT) stabilization energies of eight representative PTCDA monolayers. BSSE corrections are also shown for each structure. For the ease of comparison, energies for the MON8 structure, containing a single molecule in the unit cell, were doubled.

Phase	Square	Herringbone						Brick wall	Domino
Index	MON1	MON2	MON3	MON4	MON5	MON6	MON7	MON8	MON9
E_{stab} (eval.)	−1.00	−1.00	−1.10	−1.10	−0.72	−0.78	−0.70	−1.04	−1.08
E_{stab} (calc.)	−1.19	−1.17	−1.19	−1.34	−0.7	−1.01	−0.61	−0.89	−1.15
E_{BSSE}	0.42	0.40	0.42	0.58	0.28	0.47	0.26	0.50	0.38

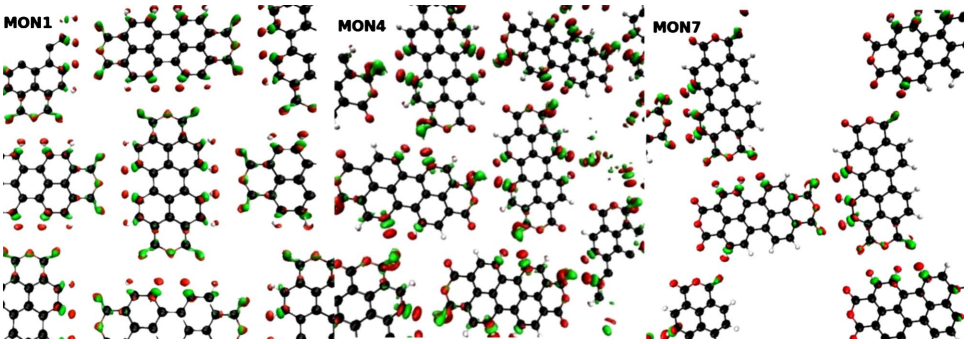

FIG. 7. (Color online) The electron density difference plots for three PTCDA monolayers, MON1, MON4, and MON7, with the contours corresponding to ± 0.01 electron/Å^3. The green surface corresponds to the regions of positive electron difference (excess) and the red areas correspond to the regions of negative electrons density difference (depletion).

The low density monolayer MON7 has very large lattice vectors and has never been observed, most likely, due to its relatively low stability. The brick wall monolayer MON8 in the gas phase, as calculated by us, has noticeably different lattice vectors as compared to those observed on the (corrugated) Ag(110) surface.[35] Finally, the MON9 structure have rather similar geometrical characteristics with the observed in this work domino phase shown in Fig. 2(b). The discrepancies between the two geometries may be explained by the effect of the substrate.

4. Going beyond the two molecules per cell

The hexagonal structure seen in Ref. 24 has not appeared in our analysis above. This is because so far we have limited ourselves to structures based on only two molecules in the unit cell. However, this particular hexagonal structure, containing four molecules in the unit cell, can be obtained by placing parallel to each other two different chains, namely F1 and F6 from Fig. 4, and then repeating the arrangement periodically in a sequence …-F1-F6-F1-F6-…. Therefore, this hexagonal structure would necessarily be considered (alongside other possible arrangements) if our method was applied with the assumption of four molecules in the cell.

One question still remains, however: it is not *a priori* obvious that such an arrangement of the chains in question would be stable. In order to check this point, we built the corresponding 2D arrangement with four molecules in the unit cell by alternating the chains F1 and F6, and relaxed it using our DFT method. The relaxed structure and its geometrical characteristics are shown in Fig. 8. One can recognize both types of chains there. Namely, looking from the top, we see F6-F1-F6-F1 sequence in the picture. However, either of the chains is distorted from their original geometry (seen in Fig. 4). This finding seem to indicate that the hexagonal structure seen in (Ref. 24) may have been additionally stabilized by the interaction with the Si/Ag(111) surface. Note that the observed there distance between equivalent molecules along the rows of 23.03 Å (Ref. 24) agrees well with the length of the lattice vector $\mathbf{A}_2$ found for the structure in our calculations.

Interestingly, the stabilization energy for this structure found in our DFT calculations (−1.14 eV with respect to two molecules) differs very little from the stabilization energies of other structures shown in Table III. This result may explain why the three phases (herringbone, square, and hexagonal) coexist on the Si/Ag(111) surface.[24]

Similarly, we can rationalize the complex structure seen in our STM image of Fig. 2(a). In this image one can notice three regions: in the region on the right and on the left a herringbone phase is clearly visible, while in the region between them (as indicated by the arrow at the top) a narrow stripe of the square phase exists. The two borders between the square and the herringbone phases are provided by exactly the same two rows F1 and F6 as in the hexagonal phase discussed above [which was, however, observed on a different Ag/Si(111) surface]. By alternating these two rows, the hexagonal phase appears. However, since one can repeat identical rows as well, as follows from our calculations on two molecules per cell structures as described in the previous subsection, these two chains provide a perfect arrangement for the herringbone phase to go continuously into the square phase and then back to the herringbone one. The particular key to the sequence seen in our STM image may be assigned as …-F6-F6-F1-F1-F1-F6-F6-… assuming that the square

TABLE IV. Geometrical characteristics of some of the experimentally observed PTCDA monolayers, including the data obtained in this work for the Au(111) surface. See Table V for the explanation of the notations. In some cases the corresponding data were missing in the quoted papers and hence was obtained directly from their images.

Phase	Square		Herringbone						Brick wall	Domino
Substrate	Si/Ag(111)	Au(111)	Si/Ag(111)	Cu(111)	Au(111)		Ag(111)	KBr(001)	Ag(110)	Au(111)
Reference	24	This work	24	34	20	This work	35	43	35	this work
A_1	16.4	17.0	20.01	21.6	20.0	19.4	19.0	19.91	17.31	15.5
A_2	16.4	17.0	11.55	13.6	12.0	12.5	12.6	11.96	16.33	15.3
γ	90.6	88	90	90	90	88	89	90	90	105
τ	90	88	88.4	90	86	85	80	83.2	0	90

TABLE V. The lengths (in Å) of the two lattice vectors and the angle γ between them (in degrees) for the selected eight PTCDA monolayers. The difference in the orientations of the two molecules within the cell are shown by the angle τ (also in degrees).

Phase	Square	Herringbone						Brick wall	Domino
Index	MON1	MON2	MON3	MON4	MON5	MON6	MON7	MON8	MON9
A_1	16.56	17.3	20.1	19.6	23.13	22.28	22.32	19.54	16.91
A_2	16.26	15.5	12.74	12.71	13.78	12.41	16.72	15.6	16.19
γ	90.1	89.6	87.6	90.1	102.1	96.7	108.0	90	90.1
τ	90	87.6	89.8	79.6	88.6	79.6	87.9	0	90

type row F1 is repeated exactly three times. This assignment is approximate due to relaxation of the molecules at the boundaries. Each particular arrangement is a result of a complicated kinetics which governs the formation of the assemblies during the deposition and (possible) further treatment.

IV. DISCUSSIONS AND CONCLUSIONS

In this paper, we have followed a systematic theoretical approach in constructing 1D and 2D planar periodic PTCDA assemblies. Our method is based on identifying all possible connections between the molecules (dimers) which enable them to form structures in the 2D gas phase. In the next step we relaxed the structures using an *ab initio* method and obtained the structures which are most energetically favorable. We find it extremely useful to study density difference plots for every structure investigated as a convenient analytical tool for assessing the strengths of various hydrogen bonds involved.

Using our theoretical method, we find a large number of 1D and 2D structures for PTCDA molecules. Our calculations show that the chains and the monolayers based on PTCDA dimers are very similar in energy and in many cases also in geometry. However, the most stable PTCDA monolayer was definitely found, MON4, shown in Fig. 5, in which the geometry of the system allows for the formation of more hydrogen bonds. Three of the obtained monolayers have been already observed experimentally as the square,[24,33–37,41] herringbone,[24,36,37,41–44] and brick wall[35,47] phases. Some other structures we find theoretically have not yet been observed. In fact, they may never been identified due to their similarity to one of the structures already observed; at the same time, some of the structures have relatively small stabilization energies and hence the probability of their formation is low.

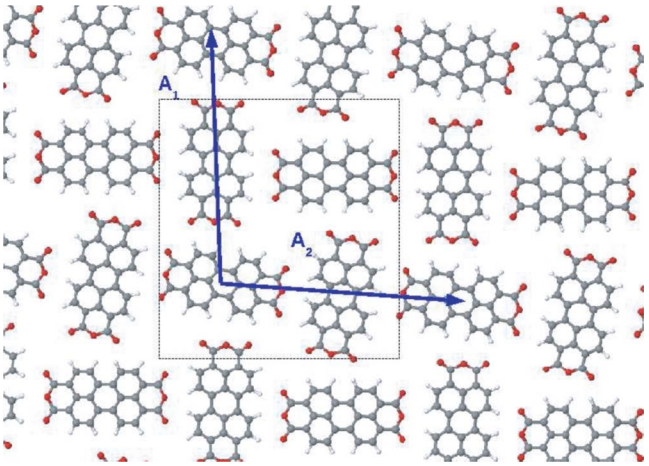

FIG. 8. (Color online) The DFT relaxed geometry of the hexagonal phase based on the PTCDA tetramer unit cell. Both the lattice vectors, $\mathbf{A}_1$ and $\mathbf{A}_2$, and the unit cell are indicated ($|\mathbf{A}_1|=23.51$ Å, $|\mathbf{A}_2|=23.35$ Å, $\gamma=83.6°$).

In parallel, we also report our STM observations of the PTCDA assemblies on the Au(111) surface. The square and domino phases on the Au(111) surface are new. The square phase can form an antiphase bonding layer between two herringbone domains, whose phases are shifted with respect to each other. That shift would depend on the width (i.e., the number of rows) of the intermediate square phase separating the two herringbone phases. Our theoretical analysis helps to rationalize this structure (as well as the previously observed on the Ag/Si(111) surface hexagonal phase), and explains why such a boundary between the two distinct phases is *not* energetically prohibitive.

A detailed comparison between theory and experiment must take into account a number of factors. Many experimental studies reported incommensurability of the molecular structures with respect to the periodicity of the substrates leading in some cases to very large cell extensions needed to match the lattice vectors of the surface (see, e.g., Refs. 24 and 34). In addition experimental observations reveal that the geometries of the same types of structures differ depending of the surfaces, e.g., various herringbone phases seen on the (111) terminations of Cu,[34] Au,[20] and Ag.[35] The effect of the substrate may be significant in some cases discussed above (e.g., for the hexagonal phase discussed in Sec. III C 4) and hence may render some of the structures we find theoretically to be unfavorable on a given substrate. These factors indicate the role played by substrate in some cases, in providing a platform for the molecules arrangements. A direct comparison of calculations and experimental STM (AFM) images would therefore require taking into account the interaction of the molecules with the surface directly, i.e., going beyond the gas-phase model adopted here. This is made even more difficult by the incommensurability problem and inability of commonly used density functionals to account for the dispersion interaction which may play a significant role in binding molecules on some surfaces such as e.g., the Au(111) surface.[74] A complete theoretical study which would take

into account all these factors is still prohibitively expensive computationally.

Nevertheless, as has been discussed in Ref. 74 in great detail, the theoretical analysis for the Au(111) surface can be significantly simplified due to the fact that the potential energy surfaces for many flat organic molecules including PTCDA are very flat. This means that the gas-phase analysis can be performed for the assemblies which effectively take account of the presence of the surface by constraining the molecules to lie in flat 2D geometries. This study provides evidence that theoretical calculations performed in the gas phase are extremely useful, at least as a first approximation, for assessing the energetics and arrangements of two-dimensional supramolecular architectures on some surfaces where intermolecular interaction dominates the molecule-surface interaction, or if the latter has a relatively small corrugation across the surface. The information on molecular energetics and possible arrangements is essential to tailor and engineer molecular assemblies at the molecular level in order to build sophisticated organic structures suitable for nanotechnology.

ACKNOWLEDGMENT

M.M. would like to thank for the computer time allocation on the HPCx and HECToR U.K. National facilities via the Material Chemistry consortium, and the financial support from the EPSRC, Grant No. GR/S97521/01. X.S. acknowledges a Bernoulli Fellowship from the University of Groningen. F.S. acknowledges financial support from Cnano Region Ile de France and from Triangle de la Physique.

*fabien.silly@cea.fr
†lev.kantorovitch@kcl.ac.uk

[1] Y. Yang and C. Wang, Chem. Soc. Rev. **38**, 2576 (2009).
[2] J. V. Barth, Annu. Rev. Phys. Chem. **58**, 375 (2007).
[3] L. Sánchez, R. Otero, J. M. Gallego, R. Miranda, and N. Martin, Chem. Rev. **109**, 2081 (2009).
[4] M. Lackinger and W. M. Heckl, Langmuir **25**, 11307 (2009).
[5] J. A. A. W. Elemans, S. Lei, and S. D. Feyter, Angew. Chem., Int. Ed. **48**, 7298 (2009).
[6] J. A. Theobald, N. S. Oxtoby, M. A. Phillips, N. R. Champness, and P. H. Beton, Nature (London) **424**, 1029 (2003).
[7] F. Silly, A. Q. Shaw, G. A. D. Briggs, and M. R. Castell, Appl. Phys. Lett. **92**, 023102 (2008).
[8] C. A. Palma, J. Bjork, M. Bonini, M. S. Dyer, A. Llanes-Pallas, D. Bonifazi, M. Persson, and P. Samori, J. Am. Chem. Soc. **131**, 13062 (2009).
[9] O. Guillermet, E. Niemi, S. Nagarajan, X. Bouju, D. Martrou, A. Gourdon, and S. Gauthier, Angew. Chem., Int. Ed. **48**, 1970 (2009).
[10] P. A. Staniec, L. M. A. Perdigão, B. L. Rogers, N. R. Champness, and P. H. Beton, J. Phys. Chem. C **111**, 886 (2007).
[11] B. Calmettes, S. Nagarajan, A. Gourdon, Y. Benjalal, X. Bouju, M. Abel, L. Porte, and R. Coratger, J. Phys. Chem. C **113**, 21169 (2009).
[12] A. Schiffrin, J. Reichert, W. Auwärter, G. Jahnz, Y. Pennec, A. Weber-Bargioni, V. S. Stepanyuk, L. Niebergall, P. Bruno, and J. V. Barth, Phys. Rev. B **78**, 035424 (2008).
[13] F. Charra and J. Cousty, Phys. Rev. Lett. **80**, 1682 (1998).
[14] R. Viswanathan, J. A. Zasadzinski, and D. K. Schwartz, Nature (London) **368**, 440 (1994).
[15] L.-M. Chen, Z. Hong, G. Li, and Y. Yang, Adv. Mater. **21**, 1434 (2009).
[16] Y. Guo, C.-A. Di, S. Ye, X. Sun, J. Zheng, Y. Wen, W. Wu, G. Yu, and Y. Liu, Adv. Mater. **21**, 1954 (2009).
[17] F. D'Souza and O. Ito, Chem. Commun. (Cambridge) **2009**, 4913.
[18] F. Rosei, M. Schunack, Y. Naitoh, P. Jiang, A. Gourdon, E. Laegsgaard, I. Stensgaard, C. Joachim, and F. Besenbacher, Prog. Surf. Sci. **71**, 95 (2003).
[19] H. Derouiche, J. C. Bernede, and J. L'Hyver, Dyes Pigm. **63**, 277 (2004).
[20] F. Silly, U. K. Weber, A. Q. Shaw, V. M. Burlakov, M. R. Castell, G. A. D. Briggs, and D. G. Pettifor, Phys. Rev. B **77**, 201408(R) (2008).
[21] M. Treier, M.-T. Nguyen, N. V. Richardson, D. Pignedoli, C. Passerone, and R. Fasel, Nano Lett. **9**, 126 (2009).
[22] F. Silly, A. Q. Shaw, K. Porfyrakis, G. A. D. Briggs, and M. R. Castell, Appl. Phys. Lett. **91**, 253109 (2007).
[23] K. J. Franke, G. Schulze, N. Henningsen, I. Fernandez-Torrente, J. I. Pascual, S. Zarwell, K. Rück-Braun, M. Cobian, and N. Lorente, Phys. Rev. Lett. **100**, 036807 (2008).
[24] J. C. Swarbrick, J. Ma, J. A. Theobald, N. S. Oxtoby, J. N. O'Shea, N. R. Champness, and P. H. Beton, J. Phys. Chem. B **109**, 12167 (2005).
[25] M. Li, K. Deng, S.-B. Lei, Y.-L. Yang, T.-S. Wang, Y.-T. Shen, C.-R. Wang, Q.-D. Zeng, and C. Wang, Angew. Chem., Int. Ed. **47**, 6717 (2008).
[26] J. C. Swarbrick, B. L. Rogers, N. R. Champness, and P. H. Beton, J. Phys. Chem. B **110**, 6110 (2006).
[27] J. Ma, B. L. Rogers, M. J. Humphry, D. J. Ring, G. Goretzki, N. R. Champness, and P. H. Beton, J. Phys. Chem. B **110**, 12207 (2006).
[28] L. Piot, F. Silly, L. Tortech, Y. Nicolas, P. Blanchard, J. Roncali, and D. Fichou, J. Am. Chem. Soc. **131**, 12864 (2009).
[29] L. Chen, W. Chen, H. Huang, H. L. Zhang, J. Yuhara, and A. T. S. Wee, Adv. Mater. **20**, 484 (2008).
[30] J. M. MacLeod, O. Ivasenko, C. Fu, T. Taerum, F. Rosei, and D. F. Perepichka, J. Am. Chem. Soc. **131**, 16844 (2009).
[31] M. D. Bonifazi, A. Kiebele, M. Stöhr, F. Cheng, T. Jung, F. Diederich, and H. Spillmann, Adv. Funct. Mater. **17**, 1051 (2007).
[32] R. R. Lunt, J. B. Benziger, and S. R. Forrest, Adv. Mater. (unpublished).
[33] M. Gabriel, M. Stöhr, and R. Möller, Appl. Phys. A: Mater. Sci. Process. **74**, 303 (2002).
[34] T. Wagner, A. Bannani, C. Bobisch, H. Karacuban, and R. Moller, J. Phys.: Condens. Matter **19**, 056009 (2007).
[35] K. Glöckler, C. Seidel, A. Soukopp, M. Sokolowski, E. Umbach,

M. Böhringer, R. Berndt, and W.-D. Schneider, Surf. Sci. **405**, 1 (1998).
[36] L. Kilian, A. Hauschild, R. Temirov, S. Soubatch, A. Schöll, A. Bendounan, F. Reinert, T.-L. Lee, F. S. Tautz, M. Sokolowski, and E. Umbach, Phys. Rev. Lett. **100**, 136103 (2008).
[37] S. Mannsfeld, M. Toerker, T. Schmitz-Hübsch, F. Sellam, T. Fritz, and K. Leo, Org. Electron. **2**, 121 (2001).
[38] J. Kröger, H. Jensen, R. Berndt, R. Rurali, and N. Lorente, Chem. Phys. Lett. **438**, 249 (2007).
[39] T. Schmitz-Hübsch, T. Fritz, F. Sellam, R. Staub, and K. Leo, Phys. Rev. B **55**, 7972 (1997).
[40] P. Fenter, F. Schreiber, L. Zhou, P. Eisenberger, and S. R. Forrest, Phys. Rev. B **56**, 3046 (1997).
[41] I. Chizhov, A. Kahn, and G. Scoles, J. Cryst. Growth **208**, 449 (2000).
[42] N. Nicoara, E. Romani, J. Gomez-Rodriguez, J. Martin-Gago, and J. Mendez, Org. Electron. **7**, 287 (2006).
[43] T. Kunstmann, A. Schlarb, M. Fendrich, Th. Wagner, R. Möller, and R. Hoffmann, Phys. Rev. B **71**, 121403(R) (2005).
[44] T. Fendrich, M. Kunstmann, D. Paulkowski, and R. Moller, Nanotechnology **18**, 084004 (2007).
[45] S. A. Burke, W. Ji, J. M. Mativetsky, J. M. Topple, S. Fostner, H.-J. Gao, H. Guo, and P. Grütter, Phys. Rev. Lett. **100**, 186104 (2008).
[46] S. A. Burke, J. M. LeDue, J. M. Topple, S. Fostner, and P. Grütter, Adv. Mater. **21**, 2029 (2009).
[47] P. Lauffer, K. Emtsev, R. Graupner, T. Seyller, and L. Ley, Phys. Status Solidi **245**, 2064 (2008).
[48] H. Huang, S. Chen, X. Gao, W. Chen, and A. T. S. Wee, ACS Nano **3**, 3431 (2009).
[49] Q. H. Wang and M. C. Hersam, Nat. Chem. **1**, 206 (2009).
[50] N. Nicoara, O. Custance, D. Granados, J. M. Garcia, J. M. Gomez-Rodriguez, A. M. Baro, and J. Mendez, J. Phys.: Condens. Matter **15**, S2619 (2003).
[51] R. Forker, T. Dienel, T. Fritz, and K. Müllen, Phys. Rev. B **74**, 165410 (2006).
[52] G. Binnig, H. Rohrer, C. Gerber, and E. Weibel, Phys. Rev. Lett. **50**, 120 (1983).
[53] G. Binnig and H. Rohrer, Rev. Mod. Phys. **59**, 615 (1987).
[54] F. Silly, A. Q. Shaw, M. R. Castell, G. A. D. Briggs, M. Mura, N. Martsinovich, and L. Kantorovich, J. Phys. Chem. C **112**, 11476 (2008).
[55] G. Binnig, K. H. Frank, H. Fuchs, N. Garcia, B. Reihl, H. Rohrer, F. Salvan, and A. R. Williams, Phys. Rev. Lett. **55**, 991 (1985).
[56] R. E. A. Kelly and L. N. Kantorovich, J. Mater. Chem. **16**, 1894 (2006).
[57] M. Mura, N. Martsinovich, and L. Kantorovich, Nanotechnology **19**, 465704 (2008).
[58] M. Mura, F. Silly, G. A. D. Briggs, M. R. Castell, and L. N. Kantorovich, J. Phys. Chem. C **113**, 21840 (2009).
[59] F. Silly, J. Microsc. **236**, 211 (2009).
[60] D. Sánchez-Portal, P. Ordejon, E. Artacho, and J. Soler, Int. J. Quantum Chem. **65**, 453 (1997).
[61] J. M. Soler, E. Artacho, J. D. Gale, A. García, J. Junquera, P. Ordejon, and D. Sanchez-Portal, J. Phys.: Condens. Matter **14**, 2745 (2002).
[62] N. Troullier and J. L. Martins, Phys. Rev. B **43**, 1993 (1991).
[63] L. Kleinman, Phys. Rev. B **21**, 2630 (1980).
[64] J. P. Perdew, K. Burke, and M. Ernzerhof, Phys. Rev. Lett. **77**, 3865 (1996).
[65] R. E. A. Kelly, Y. Lee, and L. N. Kantorovich, J. Phys. Chem. B **109**, 22045 (2005).
[66] F. Boys and F. Bernardi, Mol. Phys. **19**, 553 (1970).
[67] R. Otero, M. Schöck, L. M. Molina, E. Laegsgaard, I. Stensgaard, Bjork Hammer, and F. Besenbacher, Angew. Chem., Int. Ed. **44**, 2270 (2005).
[68] R. E. A. Kelly, M. Lukas, L. N. Kantorovich, R. Otero, W. Xu, M. Mura, E. Laegsgaard, I. Stensgaard, and F. Besenbacher, J. Chem. Phys. **129**, 184707 (2008).
[69] R. E. A. Kelly, Y. Lee, and L. N. Kantorovich, J. Phys. Chem. B **109**, 11933 (2005).
[70] R. E. A. Kelly, Y. Lee, and L. N. Kantorovich, J. Phys. Chem. B **110**, 2249 (2006).
[71] R. E. A. Kelly, W. Xu, M. Lukas, R. Otero, M. Mura, Y.-J. Lee, E. Laegsgaard, I. Stensgaard, L. N. Kantorovich, and F. Besenbacher, Small **4**, 1494 (2008).
[72] W. Xu, R. E. A. Kelly, H. Gersen, E. Laegsgaard, I. Stensgaard, L. N. Kantorovich, and F. Besenbacher, Small **5**, 1952 (2009).
[73] W. Xu, M. Dong, H. Gersen, E. Rauls, S. Vázquez-Campos, M. Crego-Calama, D. N. Reinhoudt, I. Stensgaard, E. Laegsgaard, T. R. Linderoth, and F. Besenbacher, Small **3**, 854 (2007).
[74] M. Mura, A. Gulans, T. Thinhauser, and L. Kantorovich, Phys. Chem. Chem. Phys.
[75] J. Ziroff, P. Gold, A. Bendounan, F. Forster, and F. Reinert, Surf. Sci. **603**, 354 (2009).
[76] S. Piana and A. Bilic, J. Phys. Chem. B **110**, 23467 (2006).
[77] L. Kantorovich, T. Trevethan, J. Polesel-Maris, and A. Foster, Self Consistent Image Force Interaction+virtual AFM machine.
[78] D. C. Langreth, B. I. Lundqvist, S. D. Chakarova-Kack, V. R. Cooper, M. Dion, P. Hyldgaard, A. Kelkkanen, J. Kleis, Lingzhu Kong, Shen Li, P. G. Moses, E. Murray, A. Puzder, H. Rydberg, E. Schroder, and T. Thonhauser, J. Phys.: Condens. Matter **21**, 084203 (2009).
[79] A. Gulans, M. J. Puska, and R. M. Nieminen, Phys. Rev. B **79**, 201105(R) (2009).
[80] R. Otero, M. Lukas, R. E. A. Kelly, W. Xu, E. Laegsgaard, I. Stensgaard, L. N. Kantorovich, and F. Besenbacher, Science **319**, 312 (2008).
[81] L. M. A. Perdigão, N. R. Champness, and P. H. Beton, Chem. Commun. (Cambridge) **2006**, 538.
[82] L. M. A. Perdigão, E. W. Perkins, J. Ma, P. A. Staniec, B. L. Rogers, N. R. Champness, and P. H. Beton, J. Phys. Chem. B **110**, 12539 (2006).